In Proc of Direct Methanol Fuel Cell Symposium, 199th Electrochem.l Soc. Mtg, Washington DC, 3/01.

MATHEMATICAL MODELING OF LIQUID-FEED DIRECT METHANOL FUEL CELLS

Z. H. Wang and C. Y. Wang
Electrochemical Engine Center, and Department of Mechanical and Nuclear Engineering
The Pennsylvania State University, University Park, PA 16802

A two-phase, multicomponent model has been developed for liquid-feed direct methanol fuel cells (DMFC). Diffusion and convection of both gas and liquid phases are considered in the backing layer and flow channel as well as the anode and cathode electrochemical reactions. In particular, the model fully accounts for the mixed potential effects of methanol oxidation at the cathode as a result of methanol crossover caused by diffusion, convection and electro-osmosis. The comprehensive model is solved numerically using computational fluid dynamics (CFD). The transport phenomena and electrochemical kinetics in a liquid-feed DMFC are discussed in detail and the effects of methanol concentration in the anode feed on cell performance are explored. The model is validated against limited DMFC experimental data with reasonable agreement. It is found that the void fraction at the anode outlet is as high as 90% at the cell current density of $0.7A/cm^2$ for a 7cm long channel. The increase in methanol feed concentration leads to a slight decrease in cell voltage and a proportional increase in the mass-transport limiting current density for the methanol concentration below 1M. The cell voltage, however, is greatly reduced by excessive methanol crossover and the maximum current density begins to be limited by oxygen supply at the cathode when the methanol feed concentration is larger than 2M under the operating conditions considered. The oxygen depletion results from excessive parasitic oxygen consumption by methanol crossed over.

INTRODUCTION

Fuel cells promise to replace the internal combustion engine in transportation due to their higher energy efficiency and zero or ultra-low emissions, and to replace batteries for portable electronics due to potentially higher energy density and nearly zero recharge time. Hydrogen proton exchange membrane fuel cells (PEMFC) and liquid-feed direct methanol fuel cells (DMFC) are presently considered as two potential types of fuel cells for such applications. Compared to hydrogen PEMFC, DMFC has further advantages of easier fuel delivery and storage, no cooling or humidification need, and simpler design.

However, the wide application of DMFC is still hindered by two technological problems: low electro-activity of methanol oxidation on the anode and substantial methanol crossover through the polymer membrane from the anode to cathode. The cell performance is limited by anode kinetics due to its low exchange current density and high

Tafel slope[1]. Methanol crossover further causes lower open circuit voltage (OCV) and waste of fuel and hence lower energy conversion efficiency.

Much work has been focused on the anodic oxidation of methanol[2]. The mechanism of the electrocatalytic oxidation of methanol at anode was elucidated[3, 4]. Different anode catalyst structures of Pt-Ru were developed[5] and several anode catalysts other than Pt-Ru were explored[6-8]. Additionally, the effects of the anode electrochemical reaction on cell performance were experimentally studied[9-11].

Methanol crossover in DMFC has been extensively studied both experimentally and theoretically. Narayanan et al[12] and Ren et al[13] measured the methanol crossover flux with different membrane thicknesses and showed that the methanol crossover rate is inversely proportional to the membrane thickness at a given cell current density, thus indicating that the diffusion dominates the methanol transport through membrane. In addition, Ren et al[14] compared the diffusion with electro-osmotic drag processes and demonstrated the importance of the electro-osmotic drag in the methanol transport through the membrane. In their analysis, the methanol electro-osmotic drag is considered as a convection effect and the diluted methanol moves with electro-osmotically dragged water molecules. Tricoli et al[15] compared the methanol transport in two types of membranes. Ravikumar and Shukla[11] operated the liquid-feed DMFC at the oxygen pressure of 4 bars and found that the cell performance is greatly affected by methanol crossover at the methanol feed concentration greater than 2 M and this effect aggravates with the operating temperature. Wang et al[16] analyzed the chemical compositions of the cathode effluent of a DMFC with a mass spectrometer. They found that the methanol crossing over the membrane is completely oxidized to CO_2 at the cathode in the presence of Pt catalyst. Additionally the cathode potential is influenced by the mixed potential phenomenon due to simultaneous methanol oxidation and oxygen reduction as well as poisoning of Pt catalysts by methanol oxidation products. Kauranen and Skou[17] presented a semi-empirical model to describe the methanol oxidation and oxygen reduction reactions on the cathode and concluded that the oxygen reduction current is reduced in the presence of methanol oxidation due to surface poisoning.

Despite of these two problems, progress in the DMFC performance has been made steadily by several groups, e.g. Halpert et al[18] of JPL and Giner, Inc., Baldauf and Preidel[19] of Siemens, Ren et al[20] of Los Alamos National Laboratory (LANL), and Mench et al.[43, 44] of the Penn State University. A comparative study of DMFC with hydrogen PEMFC was presented most recently by the LANL group[21, 22].

While attempts continue to elucidate the fundamental electrochemical reaction mechanisms, to explore new compositions and structures of catalysts, and to develop new membranes and methods to prevent methanol crossover, important system issues on DMFC are emerging, such as water management, gas management, flow field design and optimization, and cell up-scaling for different applications. A number of physicochemical phenomena take place in liquid-feed DMFC, including species, charge, and momentum transfer, multiple electrochemical reactions, and gas-liquid two-phase flow in both anode and cathode. Carbon dioxide evolution in the liquid-feed anode results in strongly two-

phase flow, making the mechanisms of reactant supply and product removal more complicated. All these processes are intimately coupled, resulting in existence of optimal cell design and operating conditions. A good understanding of these complex, interacting phenomena is thus essential and can be most likely achieved through a combined mathematical modeling and detailed experimental approach.

Baxter et al[23] developed a one-dimensional mathematical model for a liquid-feed DMFC, mainly focused on the anode catalyst layer. A major assumption of their study is that the carbon dioxide is only dissolved in the liquid and hence their model of transport and electrochemical processes in the anode catalyst layer is a single-phase one. Using a macro-homogeneous model to describe the reaction and transport in the catalyst layer of vapor-feed anode, Wang and Savinell[24] discussed the effects of the anode catalyst layer structure on cell performance. Kulikovsky et al[25] simulated a vapor-feed DMFC with a two-dimensional model and compared the detailed current density distributions in backing, catalyst layer, and membrane separator between a conventional and a new current collectors. In another paper, Kulikovsky[26] numerically studied a liquid-feed DMFC considering methanol transport through the liquid phase and in hydrophilic pores of the anode backing. In both publications of Kulikovsky, the important phenomenon of methanol crossover was ignored. Dohle et al[27] presented a one-dimensional model for the vapor-feed DMFC and the crossover phenomenon was described. The effects of methanol concentration on the cell performance were studied. Scott et al[28-30] also developed several simplified single-phase models to study transport and electrochemical processes in liquid-feed DMFC and showed that the cell performance is limited by the slow diffusion of methanol in liquid.

In this paper, a comprehensive model for two-phase flow, multi-component transport, and detailed electrochemical reactions is presented for a liquid-feed DMFC, including electrodes, channels, and PEM separator. The model is intended to provide a useful tool for the basic understanding of transport and electrochemical phenomena in DMFC and for the optimization of cell design and operating conditions. The model is solved using CFD and validated against limited DMFC experimental performance data. The multi-dimensional transport and electrochemical processes are analyzed numerically and the effects of the anode feed methanol concentration on cell performance are studied in detail to illustrate the utility of the present model. The two-phase transport in anode and cathode, methanol crossover, as well as their effects on cell performance are explored.

MATHEMATICAL MODELING

Consider a two-dimensional direct methanol fuel cell as schematically illustrated in Figure 1. The fuel cell includes a fluid channel, a backing layer and a catalyst layer in both electrodes and a membrane separator between the two electrodes. In the present model, the catalyst layers are simplified as infinitely thin interfaces between the backing layer and membrane separator where the following two electrochemical reactions take place:

$$CH_3OH + H_2O = CO_2 + 6H^+ + 6e \qquad \text{[R1]}$$

$$O_2 + 4H^+ = 2H_2O - 4e \qquad \text{[R2]}$$

At the anode catalyst layer, methanol is oxidized via equation [R1] while both oxygen reduction and methanol oxidation take place at the cathode via equations [R2] and [R1], respectively. According to the vast experimental evidence[16], methanol crossed over is virtually totally oxidized at the cathode catalyst layer. The above electrochemical reactions can be summarized generally as

$$\sum_k S_{Ri}^k M_k^{z_k} = n_{Ri} e^- \qquad [1]$$

where k, M_k, S^k, z_k, and n_{Ri} represent the species k, chemical formula of species k, stoichiometric coefficient, charge number of species k, and the total number of electrons produced in reaction Ri, respectively. The values of n_{Ri} are equal to 6 for reaction *R1* and –4 for reaction *R2*.

A full cell can be divided into two main groups of regions: porous regions and flow channels. The porous regions include the backing and catalyst layers of two electrodes and membrane separator. The two groups of regions will be described mathematically by different models. The two-phase mixture model developed for two-phase flow and transport in the porous air cathode[31] is extended herein for all the porous regions in the liquid-feed DMFC, while a drift flux model is used to describe the two-phase flow and transport in fluid channels. Both models are elaborated below.

Porous Regions

Governing Equations[31, 32]

Continuity:

$$\frac{\partial(\varepsilon\rho)}{\partial t} + \nabla \cdot (\rho \mathbf{u}) = 0 \qquad [2]$$

Momentum conservation:

$$\mathbf{u} = -\frac{K}{\mu}\left(\nabla p + \rho_k \mathbf{g}\right) + \frac{\xi M}{\rho}\frac{\mathbf{I}_e}{F} \qquad [3]$$

Here the fluid velocity is caused by pressure gradient, gravity, and electro-osmotic drag. The first term in equation [3] is the contribution of pressure gradient and gravity to the fluid velocity described by Darcy's law and applied for single- and two-phase flows in porous media while the second term is the contribution of electro-osmotic drag which is the sum of electro-osmotic drag flux of all the species, i.e., H_2O, MeOH and H^+ in DMFC. In the equation, M is the average molecular weight of the membrane pore fluid and ξ is fluid drag coefficient, which can be expressed as, respectively,

$$M = \sum_k \chi^k M^k \qquad [3A]$$

$$\xi = \frac{\sum_k \xi^k M^k}{M} \qquad [3B]$$

Considering the diluted methanol aqueous solution, the average molecular weight, M, can be assumed equal to the water molecular weight and the fluid drag coefficient, ξ, equal to the drag coefficient of pure liquid water in the membrane. In this case, the electro-osmotic drag of diluted methanol is considered equivalent to convection effects of electro-osmotically dragged liquid water molecules as that in Ren et al's work[14].

Species Conservation:

$$\frac{\partial}{\partial t}(\varepsilon\rho C^k) + \nabla\cdot(\gamma\rho\mathbf{u}C^k) = \nabla\cdot\left(\rho_l D^k_{l,eff}\nabla C^k_l + \rho_g D^k_{g,eff}\nabla C^k_g\right) - \nabla\cdot\left[\left(C^k_l - C^k_g\right)\mathbf{j}_l\right] + \dot{m}^k \qquad [4]$$

This general species conservation equation is applicable to methanol (CH_3OH), carbon dioxide (CO_2), oxygen (O_2), and water (H_2O). Its first three terms describe the accumulation, convection and diffusion of species k, respectively. The convection term includes the electro-osmotic drag effect, as evident for equation (3) where the fluid velocity is driven by not only the pressure gradient but also the electro-osmotic drag. The diffusion term consists of diffusion through the liquid and gas phases and the effective diffusion coefficients can be expressed as, respectively,

$$D^k_{l,eff} = (\varepsilon s)^{t_l} D^k_l \qquad [4A]$$

$$D^k_{g,eff} = [\varepsilon(1-s)]^{t_g} D^k_g \qquad [4B]$$

Note that tortuosity values are assumed equal to unity except for that in the membrane which is assumed 1.8 in the present work.

The second term on the RHS of equation [4] represents species transfer caused by relative motion of liquid to gas phase under capillary action. In this term, the capillary-diffusional flux of the liquid phase, j_l, as defined in equation [20], is directly proportional

to the gradient in capillary pressure, and thus is related the surface wetting characteristics of the porous structure.

The last term in equation [4] stands for the source/sink due to electrochemical reactions. On the anode catalyst layer, there is the methanol oxidation reaction that produces the cell current density, *I*. However, on the cathode, there are two simultaneous electrochemical reactions: oxidation of methanol crossed over through the membrane and oxygen reduction. The oxygen reduction reaction current must provide not only the net cell current density (through the external circuit) but also the parasitic current density from methanol crossover, that is $I+I_p$. A universal equation of $\dot{m}^k$ to describe species consumption/production due to electrochemical reactions that is valid throughout all porous regions can be given by

$$\dot{m}^k = \frac{M^k}{F}\left\{\left[\frac{S_{R1}^k}{n_{R1}} I_p + \frac{S_{R2}^k}{n_{R2}}\left(I + I_p\right)\right]\cdot\delta\left(y - H_{cm}\right) + \frac{S_{R1}^k}{n_{R1}} I\cdot\delta\left(y - H_{ma}\right)\right\} \qquad [5]$$

where Dirac delta function used in equation [5] can be formally defined as

$$\begin{cases} \delta(y) = \begin{cases} \infty; & y = 0 \\ 0; & y \neq 0 \end{cases} \\ \int_{\infty}^{\infty} \delta(y)dy = 1 \end{cases} \qquad [6]$$

The term in front of the first Dirac delta function in equation [5] describes the source/sink of species *k* on the cathode catalyst layer, whereas the term associated with the second Dirac delta function stands for the source/sink on the anode catalyst layer. Because of nearly complete oxidation of methanol at the cathode under the very large surface overpotential, the parasitic methanol current is dictated by the crossover rate, j^{MeOH}, as follows:

$$I_p = -\frac{j^{MeOH}\Big|_{y=H_{cm}}}{6FM^{MeOH}} \qquad [7]$$

where the methanol crossover flux is given by

$$j^{MeOH}\Big|_{y=H_{cm}} = \left(\rho_l v_l C_l^{MeOH} - \rho_l \varepsilon D_l^{MeOH} \frac{\partial C_l^{MeOH}}{\partial y} \right)\Bigg|_{y=H_{cm}} \quad [8]$$

The terms on the RHS of Eq.[8] describes convection due to the pressure difference between anode and cathode chambers and electro-osmotic drag, and diffusion, respectively. It should be noted that since the convection term is a function of methanol concentration, the three contributions to the methanol crossover flux in equation [8], namely convection by the pressure gradient, convection by the electro-osmotic drag, and diffusion by the concentration gradient, are calculated specifically at the anode backing/membrane interface. The two convection contributions are calculated in accordance with equation [3].

Mixture parameters

In the governing equations [2]-[4], the mixture variables and properties are defined as[31, 32]:

Density $$\rho = \rho_l s + \rho_g (1-s) \quad [9]$$

Concentration $$\rho C = \rho_l C_l s + \rho_g C_g (1-s) \quad [10]$$

Velocity $$\rho \mathbf{u} = \rho_l \mathbf{u}_l + \rho_g \mathbf{u}_g \quad [11]$$

Kinetic density $$\rho_\kappa = \rho_l \lambda_l(s) + \rho_g \lambda_g(s) \quad [12]$$

Viscosity $$\mu = \frac{\rho_l s + \rho_g (1-s)}{(k_{rl}/\nu_l) + (k_{rg}/\nu_g)} \quad [13]$$

Diffusion coefficient $$\rho D^k = \rho_l s D_l^k + \rho_g (1-s) D_g^k \quad [14]$$

Advection correction factor $$\gamma_c = \frac{\rho(\lambda_l C_l^k + \lambda_g C_g^k)}{\rho_l s C_l^k + \rho_g (1-s) C_g^k} \quad [15]$$

Relative mobilities $$\lambda_l(s) = \frac{k_{rl}/\nu_l}{k_{rl}/\nu_l + k_{rg}/\nu_g} \quad ; \quad \lambda_g(s) = 1 - \lambda_l(s) \quad [16]$$

Individual phase velocities:

$$\rho_l \mathbf{u}_l = \mathbf{j}_l + \lambda_l \rho \mathbf{u} \quad [17]$$

$$\rho_g \mathbf{u}_g = -\mathbf{j}_l + \lambda_g \rho \mathbf{u} \qquad [18]$$

where

$$\mathbf{j}_l = \frac{\lambda_l \lambda_g K \rho}{\mu}\left[\nabla p_c + (\rho_l - \rho_g)\mathbf{g}\right] \qquad [19]$$

Constitutive Relations

The relative permeabilities for liquid and gas phases and the capillary pressure between the two phases are:

$$k_{rl} = s^3 \quad \text{and} \quad k_{rg} = (1-s)^3 \qquad [20]$$

$$p_c = \sigma \cos\theta \left(\frac{\varepsilon}{K}\right)^{1/2}\left[1.417(1-s) - 2.120(1-s)^2 + 1.263(1-s)^3\right] \qquad [21]$$

where the surface tension effects on capillary pressure is simply modified by contact angle, θ, with θ>90° for hydrophobic surfaces and θ<90° for hydrophilic surfaces.

Equilibrium Conditions

In a gas-liquid coexisting system, local thermodynamic equilibrium prevails at the phase interface. Hence, the gas phase in the anode can be considered saturated with water and methanol vapors. It thus follows that

$$C_{g,\,sat}^{H_2O} = \frac{M^{H_2O} p_v^{H_2O}(T)}{\rho_g RT} \qquad [22]$$

where $p_v^{H_2O}(T)$ is the water vapor saturation pressure obtainable from the steam table. The methanol vapor saturation pressure can be obtained from Henry's law, i.e.,

$$p_v^{MeOH} = k_H \chi_l^{MeOH} \qquad [23]$$

where χ_l^{MeOH} is the methanol molar fraction in the liquid phase and can be determined from the mass fraction for a dilute solution:

$$\chi_l^{MeOH} \approx \frac{M^{H2O}}{M^{MeOH}} C_l^{MeOH} \qquad [24]$$

Hence, the methanol mass fraction in the gas phase is given by

$$C_g^{MeOH} = \frac{M^{MeOH} p_v^{MeOH}}{\rho_g RT} \qquad [25]$$

The mass fractions of carbon dioxide in gas and liquid phases are then simply expressed as

$$C_g^{CO_2} = \frac{M^{MeOH}\left(p - p_v^{H_2O}(T) - p_v^{MeOH}\right)}{\rho_g RT} \text{ and } C_l^{CO_2} = C_{l,sat}^{CO_2} \qquad [26]$$

Finally, the liquid saturation in the anode backing layer can be calculated from

$$s = \frac{\rho_g (C^{CO_2} - C_g^{CO_2})}{\rho_l (C_{l,\,sat}^{CO_2} - C^{CO_2}) + \rho_g (C^{CO_2} - C_g^{CO_2})} \qquad [27]$$

if $C^{CO_2} \geq C_{l,sat}^{CO_2}$. When $C^{CO_2} < C_{l,sat}^{CO_2}$, s=1.

Liquid water appears in the cathode backing layer when the water vapor pressure reaches its saturated value corresponding to the operating cell temperature. Inside the two-phase zone, thermodynamic equilibrium is assumed to hold true similarly for the anode, and thus the mass fractions of water in gas and liquid phases are given by their equilibrium values, respectively. That is,

$$C_{g,\,sat}^{H_2O} = \frac{M^{H_2O} p_v^{H_2O}(T)}{\rho_g RT} \quad \text{and} \quad C_{l,\,sat}^{H_2O} = 1 \qquad [28]$$

The liquid saturation, *s*, is therefore determined from the mixture concentration of water, *C*, via the following relation:

$$s = \frac{\rho_g (C^{H_2O} - C^{H_2O}_{g,\ sat})}{\rho_l (C^{H_2O}_{l,\ sat} - C^{H_2O}) + \rho_g (C^{H_2O} - C^{H_2O}_{g,\ sat})} \qquad [29]$$

Similarly, oxygen and carbon dioxide mass concentrations in both phases are calculated from

$$C^{O_2}_{l,sat} = 0 \qquad \text{and} \qquad C^{O_2}_{g,sat} = \left[\frac{\rho_l s}{\rho_g (1-s)} + 1 \right] C^{O_2} \qquad [30]$$

$$C^{CO_2}_{l,sat} = 0 \qquad \text{and} \qquad C^{CO_2}_{g,sat} = \left[\frac{\rho_l s}{\rho_g (1-s)} + 1 \right] C^{CO_2} \qquad [31]$$

It is assumed that oxygen and carbon dioxide are insoluble in the liquid phase on the cathode side.

Within the PEM separator, the membrane is assumed to be fully hydrated with liquid, thus

$$s = 1 \qquad for \qquad H_{cm} \le y \le H_{ma} \qquad [32]$$

Fluid Channels

Governing equations

Continuity:

Due to large gas slugs present in the anode flow channel, it is more appropriate to consider a one-dimensional flow and transport model along the flow direction that is averaged over the cross section of fluid channels. A drift-flux model is thus used in the present work to describe the significant gas-liquid two-phase flow in the anode channel. Details are presented below.

For the anode channel, the continuity equations for both phases can be written as:

$$\frac{d}{dx}\left[\rho_l U_l (1-\alpha)\right] = -\frac{N_l}{H_{cA}} \qquad [33]$$

$$\frac{d}{dx}\left[\rho_g U_g \alpha\right] = -\frac{N_g}{H_{cA}} \qquad [34]$$

where U_l and U_g are phase velocities of liquid and gas phases averaged across the flow channel, respectively, and α is the void fraction (i.e. the gas volume fraction). The terms N_l and N_g stand for mass exchange fluxes of liquid and gas between the channel and backing layer. Based on the drift flux model for the two-phase flow in a channel[33, 34], one has the following relationship between the gas and liquid phase velocities:

$$U_g = C_0\left[\alpha U_g + (1-\alpha)U_l\right] + U_{gj} \qquad [35]$$

where C_0 is a distribution parameter and U_{gj} is the drift flux velocity. According to Wolk et al[34], the distribution parameter and drift flux velocity for the slug flow through rectangular channels are given by

$$C_0 = 1.35 - 0.35\sqrt{\frac{\rho_g}{\rho_l}} \qquad [36]$$

and

$$U_{gj} = \left(0.23 + 0.13\frac{H_s}{H_w}\right)\sqrt{\frac{(\rho_l - \rho_g) g_x H_w}{\rho_l}} \qquad [37]$$

Note that in equation [37] the drift flux velocity is caused by buoyancy forces of gas phase relative to liquid phase. On the other hand, the study of Triplett et al[35] showed that the homogeneous model is more accurate for the two-phase flow through micro-capillary tubes. In such a case, the two phase velocities are equal and the distribution parameter and drift-flux velocity become unity and zero, respectively, in equation [35]. Therefore, the homogeneous model is a limiting case of the drift flux model. Because two-phase flow patterns in the DMFC anode have not been fully established, all the numerical results to be presented in the following are obtained with the homogeneous flow.

Due to a relatively small fraction of liquid droplets present in the cathode flow channel, this effect is neglected in the present work. Hence only the gas flow is considered as far as hydrodynamics is concerned.

Species conservation:

For species transport in the anode flow channel, one has

$$\frac{d}{dx}\left[\rho_l U_l (1-\alpha)\overline{C}_l^k\right] = -\frac{\rho_l v_l C_l^k\Big|_{y=H_{af}} + h_{ml}^k \rho_l \left(\overline{C}_l^k - C_l^k\Big|_{y=H_{af}}\right)}{H_{cA}} \quad [38]$$

$$\frac{d}{dx}\left[\rho_g U_g \alpha \overline{C}_g^k\right] = -\frac{\rho_g v_g C_g^k\Big|_{y=H_{af}} + h_{mg}^k \rho_g \left(\overline{C}_g^k - C_g^k\Big|_{y=H_{af}}\right)}{H_{cA}} \quad [39]$$

where the RHS of equations [38] and [39] describes the species transfer rate due to fluid convection and species diffusion at the channel/backing interface. The mass transfer coefficients used in these two equations refer to a permeable surface and therefore are rather complicated. Their expressions for similar situations were developed by Irandoust and Andersson[36] for Taylor flow in a circular capillary tube of monolithic catalyst reactors. These correlations are used in the present model for DMFC as a first approximation before more relevant and accurate relations become available. Hence,

$$h_{ml}^k = Sh_l \frac{(1-\alpha)D_l^k}{H_{cA}} \quad [40]$$

$$h_{mg}^k = Sh_g \frac{\alpha D_g^k}{H_{cA}} \quad [41]$$

$$Sh_l = 1.5\times 10^{-7}\,\mathrm{Re}^{1.648}\,Sc^{0.177}\left(\frac{\delta_{film}}{H_{cA}}\right)^{-0.2338} \quad [42]$$

$$Sh_g = \frac{\delta_{film}}{H_{cA}} \quad [43]$$

where the thickness of the liquid film around a Taylor bubble in the circular capillary channel is given by

$$\frac{\delta_{film}}{H_{cA}} = 0.18\left[1-\exp\left(-3.1Ca^{0.54}\right)\right] \quad [44]$$

with the capillary number defined as

$$Ca = \frac{\mu_l \left[\alpha U_g + (1-\alpha) U_l \right]}{\sigma} \qquad [45]$$

Alternatively the mass transfer coefficients between the anode backing and channel can be simply obtained using the effective diffusion coefficient of each phase with a fully developed flow[31] in which the Sherwood number for both gas and liquid phases in equations [40] and [41] are given by

$$Sh = 2.693 \qquad [46]$$

As a first step, equations [40], [41] and [46] have been used in this work.

There is predominant gas flow through the cathode channel. As such, the species balance equation for the gas phase can be similarly written as

$$\frac{d}{dx}\left[\rho_g U_g \overline{C}_g^k\right] = -\frac{\rho_g v_g C_g^k\Big|_{y=0} + h_{mg}^k \rho_g \left(\overline{C}_g^k - C_g^k\Big|_{y=0} \right)}{H_{cC}} \qquad [47]$$

where

$$h_{mg}^k = Sh \frac{D_g^k}{H_{cC}} \qquad [48]$$

and the Sherwood number can be obtained by equation [46].

Inlet and Outlet Boundary Conditions

Along the porous portion of the inlet and outlet boundaries, no-flow and no-flux are applied; that is

$$\left.\frac{\partial p}{\partial x}\right|_{x=0} = 0, \quad \left.\frac{\partial C^k}{\partial x}\right|_{x=0} = 0, \quad \left.\frac{\partial C^k}{\partial x}\right|_{x=0} = 0 \qquad [49]$$

$$\left.\frac{\partial p}{\partial x}\right|_{x=L} = 0\,,\ \left.\frac{\partial C^k}{\partial x}\right|_{x=L} = 0\,,\ \left.\frac{\partial C^k}{\partial x}\right|_{x=L} = 0 \qquad [50]$$

At the channel inlet, velocity and species concentrations are prescribed as

$$U_g\Big|_{x=0} = U_{in,C} \qquad [51]$$

$$C_g^k\Big| = C_{g,in,C}^k \qquad [52]$$

for the gas-feed cathode fluid channel, and

$$U_l\Big|_{x=0} = U_{in,A} \qquad [53]$$

$$C_l^k\Big| = C_{l,in,A}^k \qquad [54]$$

for the liquid-feed anode fluid channel. The outlet of each flow channel features a fully developed condition.

Electrochemical Kinetics

According to Ren et al[20], methanol oxidation is a zero-order reaction when the methanol concentration is higher than 0.1 M. In this work, a Tafel kinetic equation for methanol oxidation is developed by fitting the experimental data from Ren et al[9] as follows:

$$I = I_{0,ref}^{MeOH} \exp\left(\frac{\alpha_a F}{RT}\eta_A\right) \qquad [55]$$

Tafel kinetics of first order is also employed to describe the reaction current of oxygen reduction on the cathode catalyst interface; namely,

$$I + I_p = I_{0,ref}^{O_2} \frac{(1-s)\rho_g C_g^{O_2}\Big|_{y=H_{cm}}}{\rho_{g,ref} C_{g,ref}^{O_2}} \exp\left(-\frac{\alpha_c F}{RT}\eta_C\right) \quad [56]$$

where the term (1-*s*) is used to account for the fraction of surface rendered inactive by the presence of liquid water and the parasitic current density on the left hand side of equation [56] is attributed to oxidation of methanol crossing the membrane as given by equation [7].

Cell Voltage

Once values of the anode and cathode overpotential are calculated, the cell voltage can be determined as follows:

$$V_{cell} = U_o^{O_2} - U_o^{MeOH} - \eta_A + \eta_C - I\frac{H_{mS}}{\kappa} - IR_{contact} \quad [57]$$

where $U_o^{O_2}$ and U_o^{MeOH} are the thermodynamic equilibrium potentials of oxygen reduction and methanol oxidation and their difference is not equal to the open circuit voltage because the cathode surface overpotential is non-zero even under the open circuit in order to sustain the parasitic current from methanol crossover. The proton conductivity κ is assumed to be a constant since the membrane is fully hydrated in liquid-feed DMFC. The last term in equation [57] denotes the ohmic loss due to contact resistances between mating cell components.

NUMERICAL RESULTS

Base Case

Using a CFD technique, the present model is numerically solved for a two-dimensional liquid-feed DMFC under the baseline conditions listed in Table 2.

The predicted polarization curve of the baseline case is shown in Figure 2 (i.e. Curve 1). In this simulation, anode and cathode feed flow rates correspond to the stoichiometric current densities of 1.65A/cm^2 and 1.6A/cm^2, respectively. The curve indicates much lower cell performance of a DMFC than a hydrogen PEM fuel cell, mainly because anode kinetics is much more sluggish in DMFC. Another factor contributing to the low DMFC performance, is methanol crossover to be discussed in detail in the following subsection. As a result of methanol crossover, the predicted open circuit voltage is much lower than the thermodynamic equilibrium cell voltage (i.e.,

1.21V), a phenomenon consistent with experimental observations. In addition, the cell voltage drops very fast with the current density despite that the ohmic drop in the fully hydrated membrane is quite small, say 0.15Ω cm^2 for Nafion 117. This is caused by the high Tafel slope of methanol oxidation reaction in the anode catalyst layer, i.e. 0.293V/decade at 80°C in this baseline case. Finally it is shown that the cell current density is limited at 0.809A/cm^2 by mass transport controlled by the anode feed concentration of methanol.

To elucidate the two-phase mass transport effect on cell performance, the baseline cell is also simulated by considering the liquid phase transport only in both the anode channel and backing. This hypothetical simulation was carried out using the same computer code with the liquid saturation in the anode backing and the void fraction in the anode channel deliberately setting to unity and zero, respectively, representative of only liquid phase transport in the anode. The polarization curve in this case is shown in Figure 2 as Curve 2 and indicates a limiting current density of 0.284A/cm^2. The rather low limited current density due to slow methanol diffusion in liquid can be estimated by considering the feeding methanol concentration and the anode channel and backing mass transfer resistances using the following equation:

$$I_{\lim} = 6Fj_{\max}^{MeOH} = 6F\frac{c_l^{MeOH}}{\frac{1}{h_{ml,A}^{MeOH}} + \frac{H_{bA}}{\varepsilon_{bA}D_l^{MeOH}}} \qquad [58]$$

where the mass transfer coefficient, $h_{ml,A}^{MeOH}$, can be calculated by equations [40] and [46] with a zero void fraction. The mass transfer resistance between the fluid channel and backing layer is 1.7 times of that in the backing layer with 2mm channel width while 0.6 times with 0.7mm channel width. Both the mass transfer resistances are on the same magnitude and not negligible. At the methanol feed concentration of 1M, the limiting current density is estimated by equation [58] as 0.279A/cm^2 in this baseline case of 2mm channel width cell, closely matching the numerically predicted result. This means that cell current densities higher than 1A/cm^2 that were reported in the experiments of Ren et al[21] is impossible to sustain by methanol transport through the liquid phase only. Therefore, the gas phase is an important pathway for methanol to be transported to the reaction surface. The much facilitated methanol transport through the gas phase is due to the fact that the diffusion coefficient in gas phase is nearly four orders of magnitude greater than that in liquid.

Figure 2 also shows that the cell voltage for the liquid phase case is slightly higher than that with the two-phase transport effects included. This is because the presence of the gas phase enhances the methanol transport in the anode, thereby resulting in more severe methanol crossover and hence voltage loss associated with it. Clearly, gas phase diffusion is an important mechanism that cannot be neglected in the modeling of species transport in the liquid-feed DMFC anode. Notice also the abrupt onset of the mass

transport controlled regime shown in Fig.2, which is caused by the model assumption of the methanol oxidation reaction being zero order. In other words, no concentration polarization takes place on the anode until the methanol concentration at the catalyst site decreases to zero.

In practical DMFC systems, the anode liquid is recovered through a gas-liquid separator. As such, the inlet methanol solution is saturated with dissolved CO_2, and gas bubbles would appear immediately in the anode channel as soon as a current is drawn on the cell. Figure 3 shows the axial distributions of several flow parameters in the anode channel for the cell current density of $0.71A/cm^2$. According to Fukano and Kariyasaki[37], the gravitational effect on the two-phase flow in a mini channel is negligible as compared to the surface tension, implying that the homogeneous model for the anode channel flow is more appropriate, which is used in the present simulation. Thus, the liquid phase velocity shown in Figure 3 also represents the gas phase velocity. The velocity increases along the flow direction due to volume expansion of the two-phase mixture and the almost uniform current density distribution, as discussed below, leads to a linear increase of phase velocity. At the channel outlet, the phase velocity reaches 0.024m/s, 24 times the inlet velocity, 0.001m/s.

The void fraction in the anode channel increases rapidly along the flow direction, especially in the region near the inlet as shown in Figure 3. The void fraction increases from 0% at the inlet to 80% within one seventh of the length into the channel and greater than 90% at the outlet. The void fraction greatly affects the overall mass transfer between the channel and backing layer according to equations [40], [41] and [46] since the gas phase diffusion coefficient is four orders of magnitude higher than the liquid. With the increase in void fraction, the mass transfer between the anode channel and backing is significantly augmented. As a result, the overall mass transfer resistance from the anode channel to the backing layer decreases along the flow direction, which affects the methanol supply from anode channel to the backing and then the methanol concentration distribution discussed in the following figure.

Figure 3 also shows the average methanol concentration distribution in the liquid phase of the anode channel. It decreases almost linearly from 1M to 0.6M along the flow direction due to the electrochemical consumption at the anode catalyst layer and the methanol crossover to the cathode. In DMFC, a low methanol concentration in the anode channel is required in order to minimize methanol crossover. In the present case, the stoichiometric flow ratio of methanol supply is 2.3 at anode. At this high current density, almost all the methanol lost from the anode solution is consumed for producing the cell current and there is minimal methanol crossover occurring. It should be also noted that the gas phase at the anode outlet contains a quite bit of methanol due to the combination of relatively high methanol concentration in the gas phase (obtained from equations [23]-[25]), high gas phase velocity and high void fraction. Thus recycling the gas phase methanol seems to be necessary for high fuel utilization.

Figure 4 shows the methanol concentration contours in the anode and cathode backing layers and the PEM under the same operating conditions as in Figure 3. Near the

inlet, the overall mass transfer coefficient increases steeply due to the rapid increase in the gas phase volume fraction, causing a quick increase of the methanol concentration at the channel/backing interface. In the remaining portion of the cell, the overall mass transfer coefficient varies slightly due to a relatively slow change in the void fraction within the anode channel. Thus the methanol depletion along the anode channel dominates the gradual decrease in the methanol concentration along the anode channel/backing interface. Slight methanol crossover occurs in the front portion of the cell, whereas there is virtually no methanol available near the outlet for crossover. The methanol concentration distribution in the membrane is the result of methanol transport by diffusion, electro-osmotic drag and convection. The methanol concentration in the cathode is essentially equal to zero because any methanol crossed over through the membrane is immediately oxidized into CO_2.

Figure 5 displays the current density distribution along the flow direction under the same base conditions. In accordance with Figure 4, the local current density profile features a mass transport limited region close to the outlet where the local current density is lower than that in the middle region.

Methanol Crossover

According to equations [3], [7] and [8], methanol crossover is driven by diffusion, pressure gradient driven convection, and electro-osmosis. The three contributors manifest differently under different operating conditions. Figures 6 (a) and (b) show the axial distributions of the total methanol crossover flux and its individual contributors for two cases of high and low current densities, respectively. Figure 6 (a) corresponds to the baseline cell operation with the current density of $0.71A/cm^2$. In this high cell current density case, methanol crossover appears only in the front portion of the cell, where the contributions of diffusion and electro-osmosis equally dominate while the convection contribution is almost absent due to no pressure gradient between the anode and cathode chambers. The variation of the net methanol crossover flux along the flow direction in this figure explains the local current density distribution in Figure 5.

Figure 6 (b) shows the different contributions to methanol crossover at the cell current density of $0.18A/cm^2$. In this low current density case, diffusion dominates the net methanol crossover at all locations. The contribution of electro-osmosis accounts for 15% of the net crossover flux. Compared to Figure 6 (a), the maximum diffusion flux is greatly increased from about $0.060A/cm^2$ to $0.14A/cm^2$ due to the significant increase of methanol concentration at the anode catalyst layer. Since the electro-osmotic flux is a combination of the methanol concentration and cell current density as can be seen from equation [8], it remains roughly the same in the inlet area because the methanol concentration in the membrane decreases with the current density increasing.

At open circuit, no current is drawn from the anode and the anode fluid is in liquid state. Hence methanol transport occurs only by liquid diffusion from the anode channel,

to the anode backing layer, then through the membrane separator to the cathode catalyst layer. The methanol crossover flux can thus be estimated by the following equation:

$$I_{p,oc} = 6Fj_{\max}^{MeOH} = 6F\frac{c_l^{MeOH}}{\frac{1}{h_{ml,A}^{MeOH}} + \frac{H_{bA}}{D_{l,eff,bA}^{MeOH}} + \frac{H_{mS}}{D_{l,eff,mS}^{MeOH}}} \quad [59]$$

Under the baseline conditions, the methanol crossover flux is calculated to be 0.116A/cm^2 at open circuit. This value is smaller than that of 0.133A/cm^2 at a current density of 0.18 A/cm^2, implying that the methanol transport through the gas phase upon electrochemical reaction in the anode must increase the methanol crossover rate. It should be noted that a tortuosity factor of 1.8 is used for the methanol effective diffusion coefficient in membrane.

The detrimental effect of methanol crossover on cell performance can be seen from Figure 7 that shows the polarization curves with and without methanol crossover. At small current densities, the cell voltage difference can be as high as 0.1V. This voltage loss is reduced with the current density increasing and becomes zero when the fuel cell reaches its mass transport limiting current density. At this point no methanol crosses over the membrane and all the methanol is consumed by anode oxidation. It is noted, however, that the predicted cell voltage loss due to methanol crossover as appears to be less significant than observed experimentally. Further work is needed to fully explain this.

Effects of Methanol Feed Concentration

Figure 8 shows the effects of methanol feed concentration on the polarization curves under the operating conditions listed in Table 2. The anode stoichiometric current density is calculated by 1.65×n A/cm^2, where n is the methanol feed concentration with a unit of M. Better cell performance is achieved with low feed concentrations for small current densities. This is because the small methanol concentration in the anode minimizes the rate of methanol crossover. However, operating with small feed concentrations suffers from low limiting current densities. Operation in the medium current density range requires a high methanol feed concentration although its cell voltage is low under open circuit or low current densities because of excessive methanol crossover. The polarization curves for methanol feed concentrations higher than 1M are of a different shape. In the presence of substantial methanol crossover experienced in high methanol feed concentration cases, say 4M, a significant amount of oxygen in the cathode is consumed by methanol oxidation. Different from the cases of smaller methanol feed concentration, in which the cell current density is limited by methanol mass transport, the cell current density is limited by oxygen supply at a higher methanol feed concentration. While a stoichiometric flow ratio of the oxidant is traditionally defined on the basis of the net current density of the cell for convenience, it must be

noted that the intrinsic stoichiometry of O_2 should be defined based on $(I+I_p)$. Under high current densities, the former stoichiometry is typically around 2.2, while the latter stoichiometry can be close to unity, meaning that the oxygen concentration at the outlet of the cathode is nearly zero!

Model Validation

The present model is validated by the experiment data of a 50cm^2 stainless steel cell and a 5cm^2 graphite cell. Figure 9 shows the polarization curves under two experimental conditions of the 50cm^2 cell carried out by Mench et al.[43] In order to fit the experimental data, the reference anode exchange current density at 80°C and contact resistance used in the above simulation are adjusted in this part of the paper. The figure shows that the numerical results agree well if the contact resistance is 0.35Ω cm^2 and the reference anode exchange current density is 28.3A/m^2 for 80°C. The exchange current density in the present paper is defined on the basis of the electrode cross-sectional area.

The model is also validated against the experimental data of a 5cm^2 graphite DMFC. Figure 10 shows the polarization curves at two cell temperatures. Note that the anode kinetics of this cell is measured with the corresponding MEA for this model validation and the following kinetics equation is fitted to the experimental data,

$$I = I_{0,ref}^{MeOH}\left(-0.810 + 3.26\frac{T_{ref}}{T}\eta_a\right) \qquad [60]$$

which is applied in this validation simulation. Considering that gas bubbles are not in a continuous phase, the gas diffusion coefficient is adjusted in the validation. In this case, the methanol gas diffusion coefficient is 1/6 of that in the continuous phase. The figure shows that the model predictions agree well with the experimental data. A lower mass transport limited current density at 50°C is caused by the lower diffusion coefficients in both liquid and gas phases and the lower saturated methanol concentration in the gas phase at lower temperatures as listed in Table 2.

Figure 11 shows the polarization curves of numerical and experimental results for the 5cm^2 cell at different methanol feed concentrations. In agreement with the experiments, the model prediction for the 2M case shows a lower performance, due primarily to higher methanol crossover.

CONCLUSIONS

A two-phase multicomponent model with mixed potential effects has been developed for the liquid-feed DMFC. Diffusion and convection of both gas and liquid phases are considered to understand methanol crossover through the membrane caused by diffusion, convection and electro-osmosis. The model is solved numerically using

computational fluid dynamics and validated against available experimental data. The interactive transport phenomena and electrochemical kinetics in liquid-feed DMFC are studied based on the simulation results, and the effects of methanol feed concentrations on cell performance are discussed. Gas phase transport is important in delivering methanol to the reaction site due to the much higher diffusion coefficient in the gas phase. The void fraction at the outlet can be as high as 90% and the gas and liquid phase velocities in the anode can be increased by an order of magnitude from the inlet to the outlet due to significant volume expansion. The increase in methanol feed concentration leads to a slight decrease in cell voltage and but a proportional increase in the maximum cell current density when the methanol concentration is smaller than 1M. At methanol concentrations greater than 2M the cell voltage is greatly reduced due to excessive methanol crossover and the maximum cell current density may be limited by oxygen transport on the cathode because the parasitic reaction from methanol crossover consumes oxygen as well.

Methanol crossover is dominated by molecular diffusion at zero and small current densities and the local distribution of the crossover flux is almost uniform along the channel flow direction. At high current densities, the methanol crossover flux becomes small and both the diffusion and elelctro-osmosis equally contribute to methanol crossover. The cell voltage can be reduced by 0.1V with methanol crossover at a small current density but the effect decreases with increasing cell current density. The oxidation of methanol on the cathode may cause exhaustion of oxygen, thus implying that the cathode stoichiometric flow ratio cannot be at a similarly low level to the hydrogen fuel cell not only because of the need to prevent cathode flooding but also the competing consumption of oxygen between parasitic and main cathode reactions.

LIST OF SYMBOLS

c	molar concentration, M
C	mass fraction, kg/kg
Ca	capillary number
C_0	distribution parameter
D	diffusivity, cm^2/s
F	Faraday constant, 96,487 C/mol
$\boldsymbol{g}$	gravitational acceleration, cm/s^2
H_{af}	location of anode backing/channel interface, cm
H_{bA}	thickness of anode backing layer, cm
H_{bC}	thickness of cathode backing layer, cm
H_{cA}	anode channel height, cm
H_{cC}	cathode channel height, cm
H_{cm}	location of cathode backing/membrane interface (cathode catalyst layer), cm
h_m	mass transfer coefficient between porous electrode and gas channel, cm/s
H_{ma}	location of membrane and anode backing interface (anode catalyst layer), cm
H_{mS}	membrane separator thickness, cm
H_s	length of shorter side of rectangular channel cross section, cm

H_w	length of wider side of rectangular channel cross section, cm
I	current density, A/cm^2
I_0	effective exchange current density, A/cm^2
I_p	parasitic current density at cathode resulting from methanol crossover, A/cm^2
$\mathbf{I_e}$	ionic current density vector, A/cm^2
j	species mass flux, kg/cm^2 s
K	permeability of porous material, cm^2
k_H	Henry's law constant, Pa
k_{rg}	relative permeability of gas phase
k_{rl}	relative permeability of liquid phase
L	cell length, cm
$\dot{m}$	source term in species conservation equation, kg/cm^3 s
M	molecular weight, kg/mol
M_k	formula of species k
N	mass flow rate, kg/cm^2 s
n_{Ri}	net electrode output of electrode reaction Ri
p	pressure, Pa
p_A	anode pressure, Pa
p_c	capillary pressure, Pa
p_C	cathode pressure, Pa
p_v	saturated vapor pressure, Pa
R	gas constant, J/(mol·K)
$R_{contact}$	ohmic contact resistance, Ω cm^2
Re	Reynolds number, $\frac{\rho u H}{\mu}$
RH	relative humidity
S_{Ri}^k	stoichiometric coefficient of species k in reaction Ri
Sc	Schmidt number, $\frac{\nu}{D}$
Sh	Sherwood number, $\frac{h_m H}{D}$
s	liquid saturation
t	time, s
T	temperature, K
U	phase velocity in channel, cm/s, or potential, V
$U_{g,j}$	drift velocity, cm/s
$\mathbf{u}$	superficial velocity vector, cm/s
u	velocity in x direction, cm/s
v	velocity in y direction, cm/s
V_{cell}	cell voltage, V
x	coordinate, cm
y	coordinate, cm

Greek Symbols

α	void fraction in channel
α_a	anodic transfer coefficient at anode
α_c	cathodic transfer coefficient at cathode
χ	molar fraction in liquid solution, mol/mol
δ_{film}	liquid film thickness of Taylor flow, cm
ε	porosity
η	overpotential, V
κ	ionic conductivity of membrane, cm/Ω
μ	viscosity, kg/(cm·s)
ν	kinetic viscosity, cm^2/s
θ	contact angle, °
ρ	density, kg/cm^3
ρ_k	kinetic density, kg/cm^3
σ	interfacial tension, N/cm
ξ	electro-osmotic drag coefficient per proton

Superscripts

CO_2	carbon dioxide
H_2O	water
k	species k
$MeOH$	methanol
O_2	oxygen
t_g	tortuosity factor of gas phase diffusion
t_l	tortuosity factor of liquid phase diffusion
$\bar{}$	average value in channel

Subscripts

A	anode
bA	anode backing layer
bC	cathode backing layer
C	cathode
cA	anode channel
cC	cathode channel
eff	effective value
eq	equilibrium value
g	gas phase
in	inlet
l	liquid phase
mS	membrane separator
oc	open circuit

ref reference value
sat saturated

REFERENCES

1. G. T. Burstein, C. J. Barnett, A. R. Kucernak and K. R. Williams, *Catalysis Today*, **38**, 425 (1997).
2. S. Wasmus and A. Kuver, *Journal of Electroanalytical Chemistry*, **461**, 14 (1999).
3. W. F. Lin, J. T. Wang and R. F. Savinell, *Journal of Electrochemical Society*, **144**, 1917 (1997).
4. Hamnett, *Catalysis Today*, **38**, 445 (1997).
5. S. C. Thomas, X. Ren and S. Gottesfeld, *Journal of Electrochemical Society*, **146**, 4354 (1999).
6. L. Liu, C. Pu, R. Viswanathan, Q. Fan, R. Liu, and E. S. Smotkin, *Electrochimica Acta*, **43**, 3657 (1998).
7. E. Hayden, *Catalysis Today*, **38**, 473 (1997).
8. T. Page, R. Johnson, J. Hormes, S. Noding, B. Rambabu, *Journal Electroanalytical Chemistry*, **485**, 34 (2000).
9. X. Ren, T. E. Springer, and S. Gottesfeld, *Journal of Electrochemical Society*, **147**, 92 (2000).
10. S. Arico, P. Creti, E. Modica, G. Monforte, V. Baglio, and V. Antonucci, *Electrochimica Acta*, **45**, 4319 (2000).
11. M. K. Ravikumar and A. K. Shukla, *Journal of Electrochemical Society*, **143**, 2601 (1996).
12. S. R. Narayanan, H. Frank, B. Jeffries-Nakamura, M. Smart, W. Chun, G. Halpert, J. Kosek, and C. Cropley, in *Proton Conducting Membrane Fuel Cells I*, S. Gottesfeld, G. Halpert, A. Landgrebe, Editors, PV 95-23, p. 278, The Electrochemical Society Proceedings Series, Pennington, NJ (1995).
13. X. Ren, T. A. Zawodzinski Jr., F. Uribe, H. Dai, and S. Gottesfeld, in *Proton Conducting Membrane Fuel Cells I*, S. Gottesfeld, G. Halpert, A. Landgrebe, Editors, PV 95-23, p. 284, The Electrochemical Society Proceedings Series, Pennington, NJ (1995).
14. X. Ren, T. E. Springer, T. A. Zawodzinski, and S. Gottesfeld, *Journal of Electrochemical Society*, **147**, 466 (2000).
15. V. Tricoli, N. Carretta, and M. Bartolozzi, *Journal of Electrochemical Society*, **147**, 1286 (2000).
16. J. T. Wang, S. Wasmus, and R. F. Savinell, *Journal of Electrochemical Society*, **143**, 1233 (1996).
17. P. S. Kauranen and E. Skou, *Journal of Electroanalytical Chemistry*, **408**, 189 (1996).
18. G. Halpert, S. R. Narayanan, T. Valdez, W. Chun, H. Frank, A. Kindler, S. Surampudi, J. Kosek, C. Cropley, and A. LaConti, in *Proceedings of the 32nd Intersociety Energy Conversion Engineering Conference*, Vol. 2, p. 774, AIChE, New York (1997).
19. M. Baldauf and W. Preider, *Journal of Power Sources*, **84**, 161 (1999).

20. X. Ren, P. Zelenay, S. Thomas, J. Davey, and S. Gottesfeld, *Journal of Power Sources*, **86**, 111 (2000).
21. X. Ren, M. S. Wilson and S. Gottesfeld, *Journal of Electrochemical Society*, **143**, L12 (1996).
22. S. Gottesfeld and M. S. Wilson, in *Energy Storage Systems for Electronics Devices*, T. Osaka and M. Datta, Editors, p. 487, Gordon and Breach Science Publishers, Singapore (2000).
23. S. F. Baxter, V. S. Battaglia, and R. E. White, *Journal of Electrochemical Society*, **146**, 437 (2000).
24. J. Wang and R. F. Savinell, in *Electrode Materials and Processes for Energy Conversion and Storage*, S. Srinivasan, D. D. Macdonald, A. C. Khandkar, Editors, PV 94-23, p. 326, The Electrochemical Society Proceedings Series, Pennington, NJ (1994).
25. A. Kulikovsky, J. Divisek, and A. A. Kornyshev, *Journal of Electrochemical Society*, **147**, 953 (2000).
26. A. A. Kulikovsky, *Journal of Applied Electrochemistry*, **30**, 1005 (2000).
27. H. Dohle, J. Divisek, and R. Jung, *Journal of Power Sources*, **86**, 469 (2000).
28. K. Scott, P. Argyropoulos and K. Sundmacher, *Journal of Electroanalytical Chemistry*, **477**, 97 (1999).
29. K. Sundmacher and K. Scott, *Chemical Engineering Science*, **54**, 2927 (1999).
30. P. Argyropoulos, K. Scott and W. M. Taama, *Journal of Applied Electrochemistry*, **30**, 899 (2000).
31. Z. H. Wang, C. Y. Wang, and K. S. Chen, *J. Power Sources*, **94**, 40 (2001).
32. C. Y. Wang and P. Cheng, *Advances in Heat Transfer*, **30**, 93 (1997).
33. T. Wilmarth and M Ishii, *Int. J. Heat Mass Transfer*, **37**, 1749 (1994).
34. G. Wolk, M. Dreyer, and H. J. Rath, *Int. J. Multiphase Flow*, **26**, 1037 (2000).
35. K. A. Triplett, S. M. Ghiaasiaan, S. I. Abdel-Khalik, A. leMouel, and B. N. McCord, *Int. J. Multiphase Flow*, **25**, 395 (1999).
36. S. Irandous and B. Anderson, *Computers Chem. Engng*, **13**, 519 (1989).
37. T Fukano and A. Kariyasaki, *Nuclear Engineering and Design*, **141,** 59 (1993).
38. E. L. Cussler, *Diffusion: Mass Transfer in Fluid Systems*, Cambridge University Press, New York (1984).
39. C. L. Yaws, *Handbook of Transport Property Data: viscosity, thermal conductivity, and diffusion coefficients of liquids and gases*, Gulf Pub Co., Houston, Tex (1995).
40. F. D. Incropera and D. P. DeWitt, *Fundamentals of Heat and Mass Transfer*, John Wiley & Sons, Inc., New York (1985).
41. S. Gottesfeld and T. A. Zawodzinski, *Advances in Electrochemical Science and Engineering*, **6**, 195 (1997).
42. M. L. McGlashan and A. G. Williamson, *Journal of Chemical and Engineering Data*, **21,** 196 (1976).
43. M. Mench, S. Boslet, S. Thynell, J. Scott, and C.Y. Wang, in *Direct Methanol Fuel Cells*, The Electrochemical Society Proceedings Series, Pennington, NJ (2001).
44. M. Mench, J. Scott, S. Thynell and C.Y. Wang, presented at *200th Electrochemical Society Fall Meeting*, San Francisco, Sept.2-7. Abstract No.315 (2001).

Table 1 Physicochemical properties

Parameter	Symbol	Value	Reference
Diffusion coefficient of oxygen in gas	$D_g^{O_2}$	$1.775\left(\frac{T}{273}\right)^{1.823}\left(\frac{1.013\times10^5}{P}\right)$ m^2/s	Cussler[38]
Diffusion coefficient of carbon dioxide in gas	$D_g^{CO_2}$	3×10^{-5} m^2/s	Assumed
Diffusion coefficient of carbon dioxide in liquid	$D_l^{CO_2}$	1×10^{-10} m^2/s	Assumed
Diffusion coefficient of methanol in gas	D_g^{MeOH}	$\left(\begin{array}{l}-6.954\times10^{-2}+4.5986\\ \times10^{-4}T\\ +9.4979\times10^{-7}T^2\end{array}\right)\times10^{-4}$ m^2/s	Yaws[39]
Diffusion coefficient of methanol in liquid	D_l^{MeOH}	$10^{-5.4163-\frac{999.778}{T}}$ m^2/s	Yaws[39]
Diffusion coefficient of water in gas	$D_g^{H_2O}$	$2.56\times10^{-5}\left(\frac{T}{307}\right)^{2.334}\left(\frac{1.013\times10^5}{P}\right)$ m^2/s	Cussler[38]
Diffusion coefficient of water in liquid	$D_l^{H_2O}$	0 m^2/s	Assumed
Electro-osmotic drag coefficient of water	ξ^{H_2O}	2.5	Ren et al[14]
Electro-osmotic drag coefficient of methanol	ξ^{MeOH}	$\xi^{H_2O}\chi^{MeOH}$	Ren et al[14]
Viscosity of liquid water	μ_l	$0.458509-5.30474\times10^{-3}T$ $+2.31231\times10^{-5}T^2-4.49161\times10^{-8}T^3$ $+3.27681\times10^{-11}T^4$ kg/m s	Incropera[40]
Viscosity of gas	μ_g	2.03×10^{-5} kg/m s	Incropera[40]
Permeability of anode backing layer	K	1×10^{-11} m^2	Assumed
Permeability of cathode backing layer	K	1×10^{-11} m^2	Assumed
Permeability of membrane	K	1×10^{-21} m^2	Assumed

Cathodic transfer coefficient of cathode	α_c	0.875	Fitted from Gottesfeld and Zawodzinski[41]
Anodic transfer coefficient of anode	α_a	0.239	Fitted from Ren et al[9]
Reference exchange current density of anode at 80°C	$I^{MeOH}_{0,ref,80^\circ C}$	94.25 A/m^2	Fitted from Ren et al[9]
Reference exchange current density of anode	$I^{MeOH}_{0,ref}$	$I^{MeOH}_{0,ref,80^\circ C} e^{\frac{35570}{R}\left(\frac{1}{273+80}-\frac{1}{T}\right)}$	Fitted from Gottesfeld and Wilson[22]
Reference exchange current density of cathode	$I^{O_2}_{0,ref}$	0.04222 A/m^2	Fitted from Gottesfeld and Zawodzinski[41]
Reference oxygen concentration of cathode kinetics	$C^{O_2}_{g,ref}$	0.23 kg/kg	—
Reference gas density	$\rho_{g,ref}$	1.2 kg/m^3	—
Porosity of cathode backing layer	ε_{bC}	0.7	Measured
Porosity of anode backing layer	ε_{bA}	0.7	Measured
Porosity of membrane	ε_{mS}	0.3	Measured
Henry's law constant	k^{MeOH}	$0.096e^{0.04511(T-273)}$ atm	McGlashan and Williamson[42]
Thermodynamic potential of oxygen reduction	$U^{O_2}_o$	1.24 V	—
Thermodynamic potential of methanol oxidation	U^{MeOH}_o	0.03 V	—
Proton conductivity	κ	0.123 S/cm	Ren et al[9]

Table 2 Base case and its operating conditions

Parameter	Symbol	Value
Cathode backing thickness	H_{bC}	0.03 cm
Anode backing thickness	H_{aA}	0.03 cm
PEM thickness	H_{mS}	0.0185 cm
Anode channel height	H_{cA}	0.2 cm
Cathode channel height	H_{cC}	0.2 cm
Cell length	L	7 cm
Operating temperature	T	80 °C
Cathode channel pressure	p_C	1 atm
Anode channel pressure	p_A	1 atm
Inlet velocity of cathode channel	$U_{in,\,C}$	0.2 m/s
Inlet velocity of anode channel	$U_{in,\,A}$	0.001m/s
Inlet relative humidity at cathode	RH_{in}	3.43%
Inlet oxygen concentration at cathode	$C_{g,in,C}^{O_2}$	0.23 kg/kg (0.21mol/mol)
Inlet methanol concentration at anode	$C_{l,in,A}^{MeOH}$	0.032 kg/kg (1M)
Contact resistance	$R_{contact}$	0 Ω cm^2

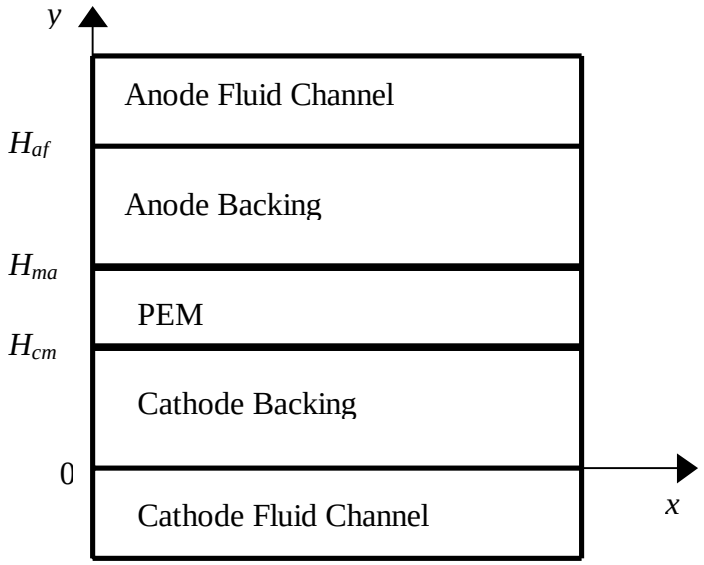

Figure 1 Schematic of a liquid-feed direct methanol fuel cell for the present model

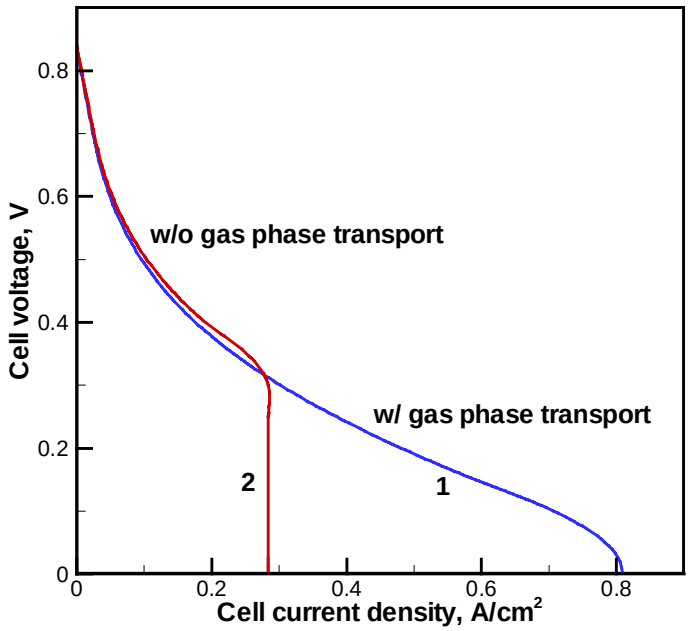

Figure 2 Polarization curves for the baseline cell with and without mass transport through gas and gas phase

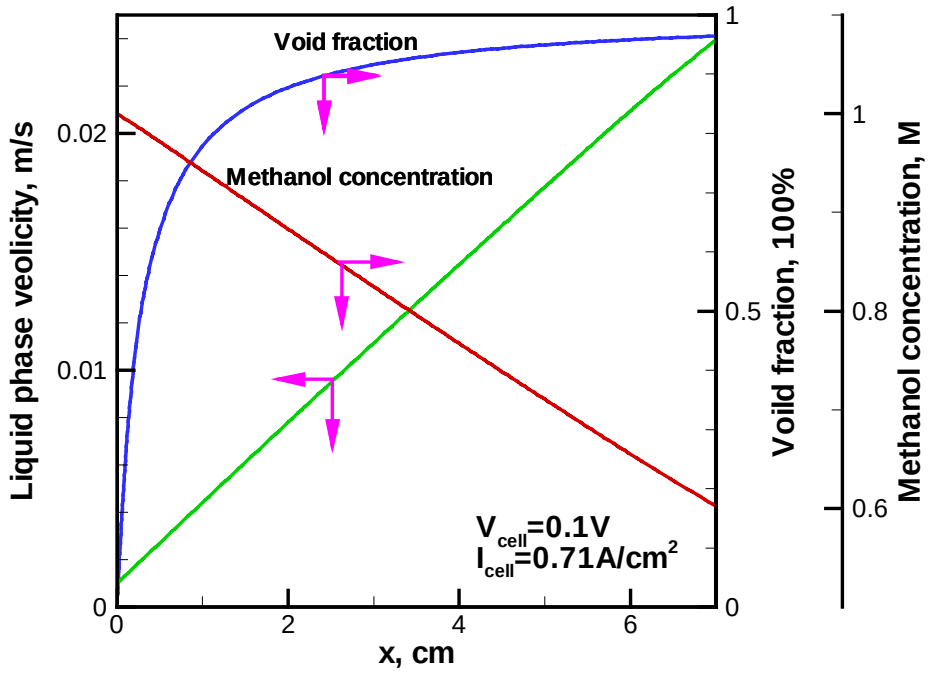

Figure 3 Axial profiles of liquid phase velocity, void fraction and average methanol concentration in the anode channel at 0.71A/cm^2.

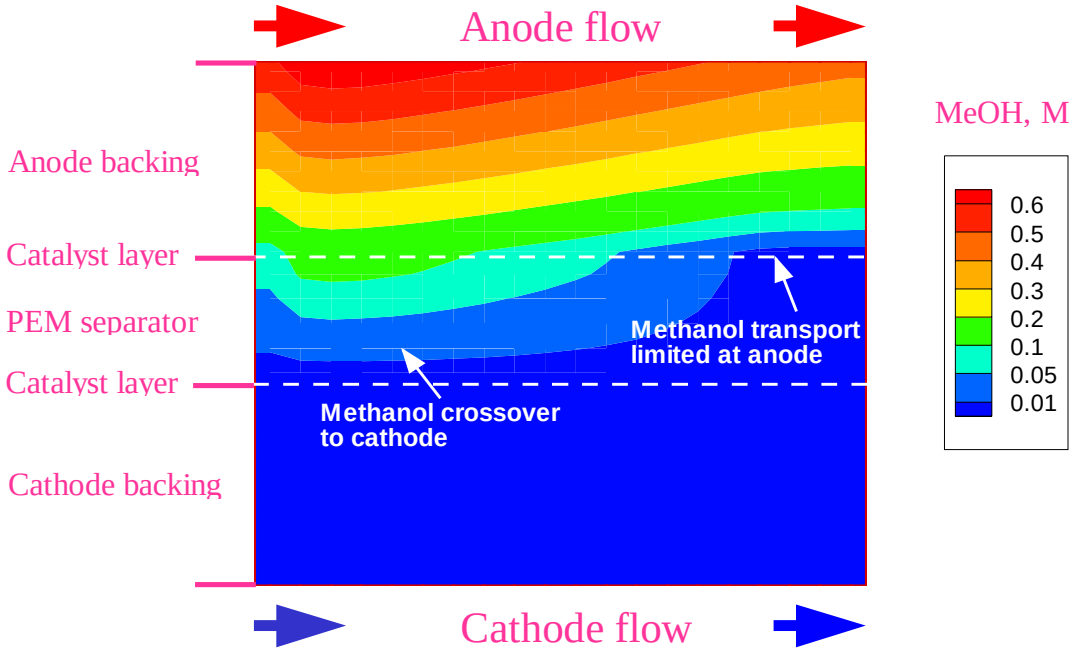

Figure 4 Methanol concentration contours in the membrane-electrode assembly for 0.71A/cm^2.

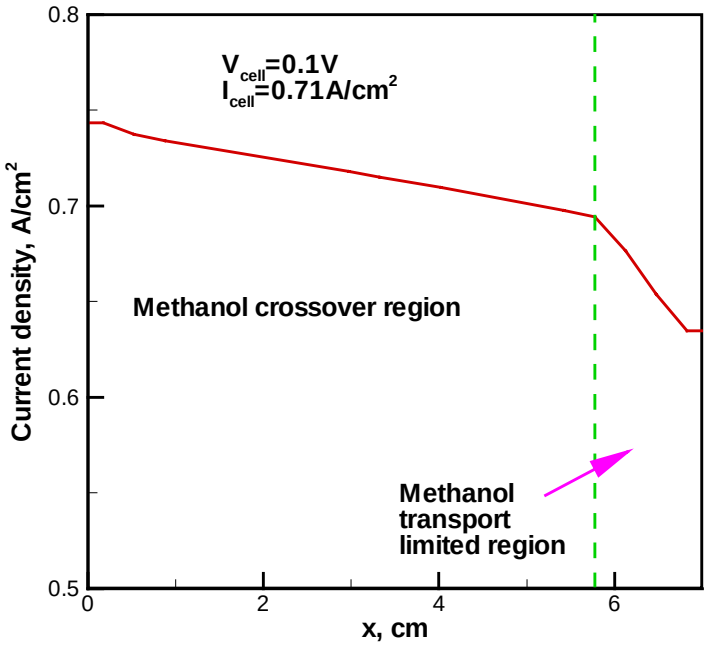

Figure 5 Local current density distribution along the flow direction for the average cell current density of 0.71A/cm^2.

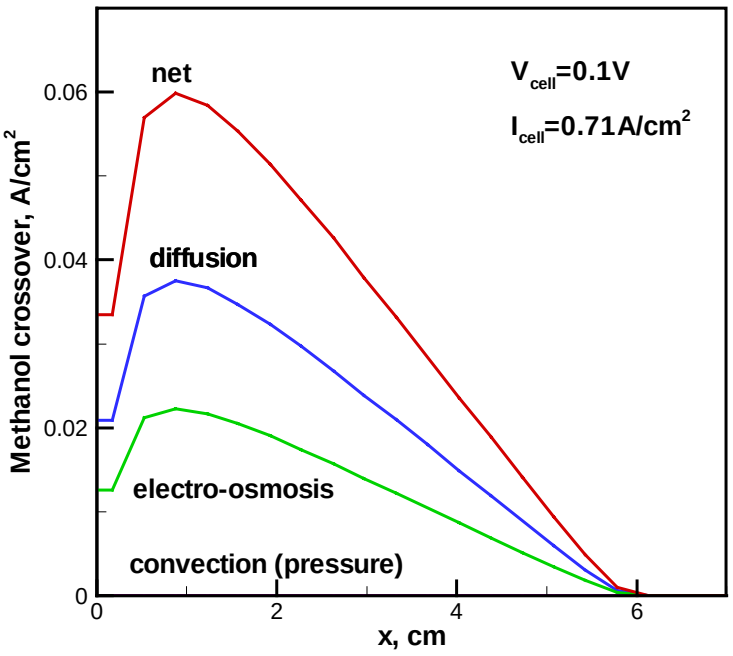

(a)

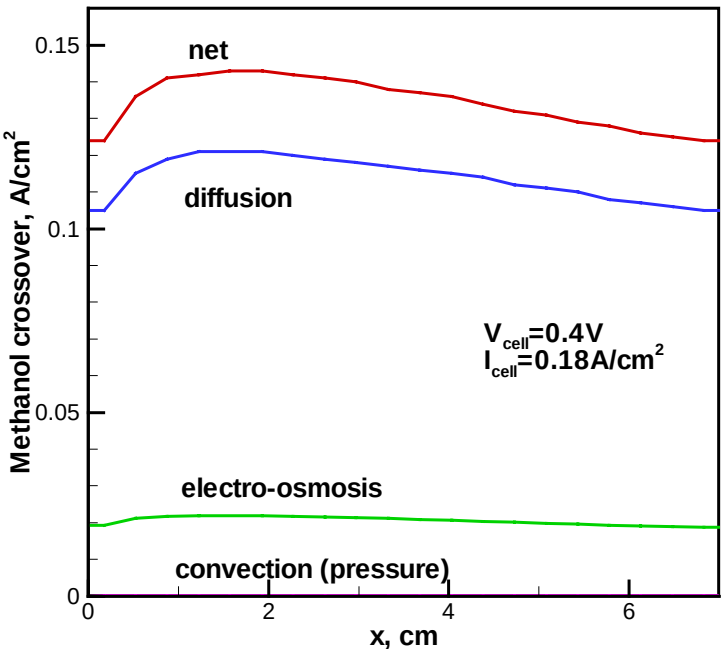

(b)

Figure 6 Axial distributions of methanol crossover flux and its contributors for (a) high current density case, and (b) low current density case.

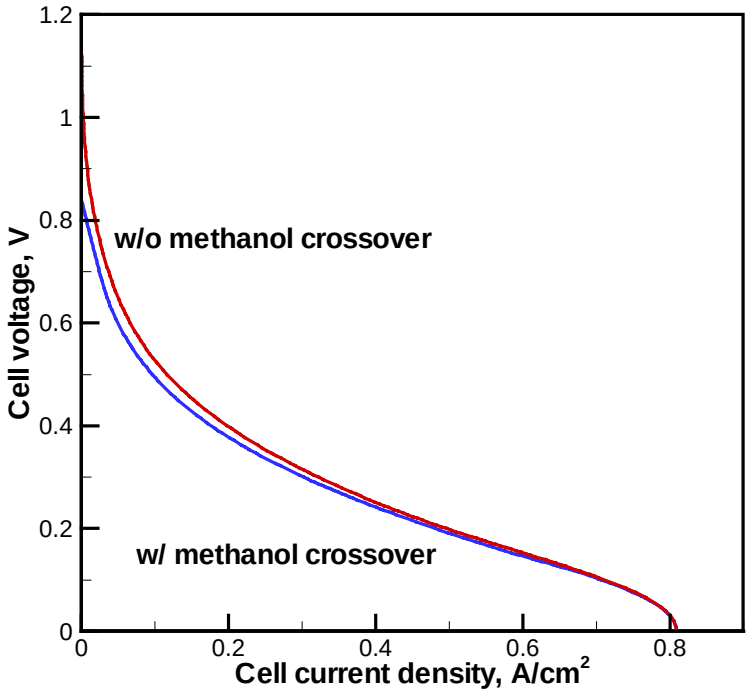

Figure 7 Polarization curves and methanol crossover effects

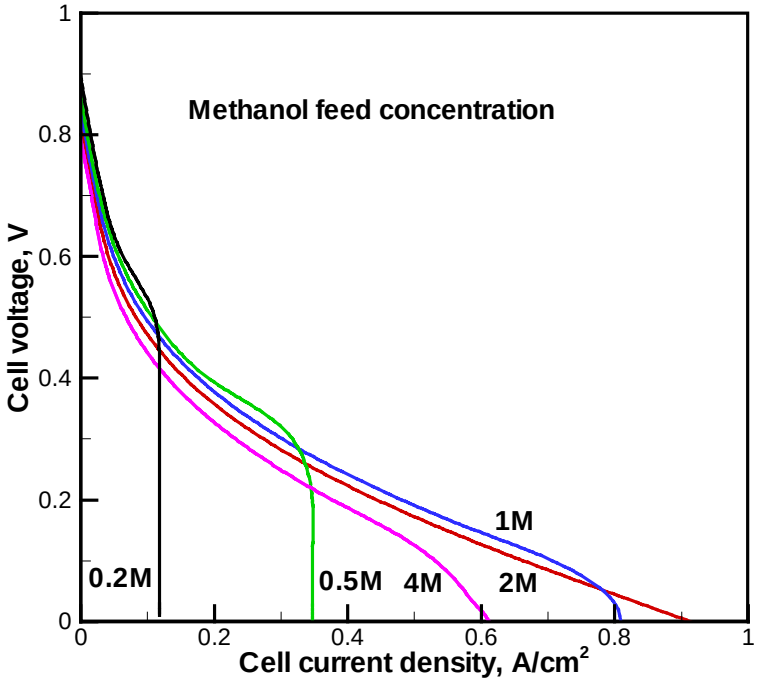

Figure 8 Polarization curves with different methanol feed concentrations.

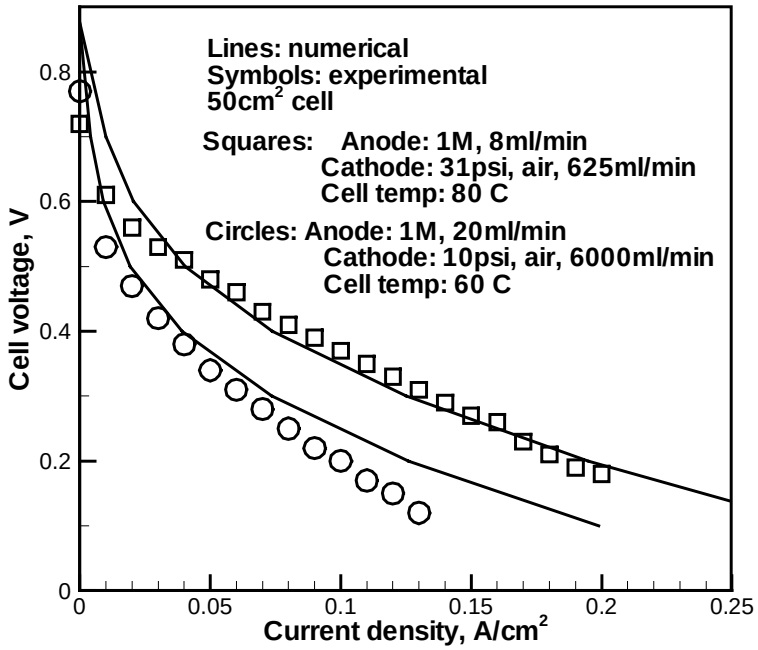

Figure 9 Validation of the present DMFC model with the experimental data of a 50cm^2 stainless steel cell at different temperatures

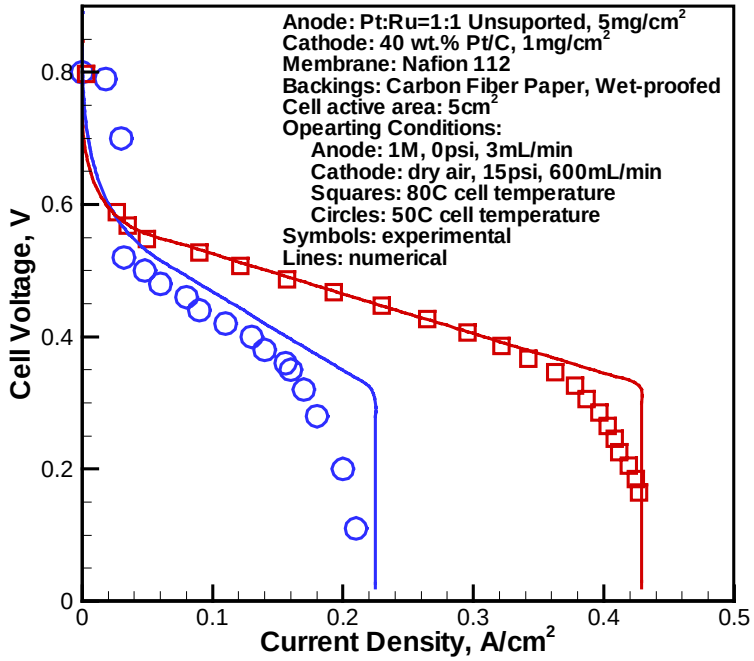

Figure 10 Validation of the present DMFC model with the experimental data of a 5cm^2 cell at different temperatures

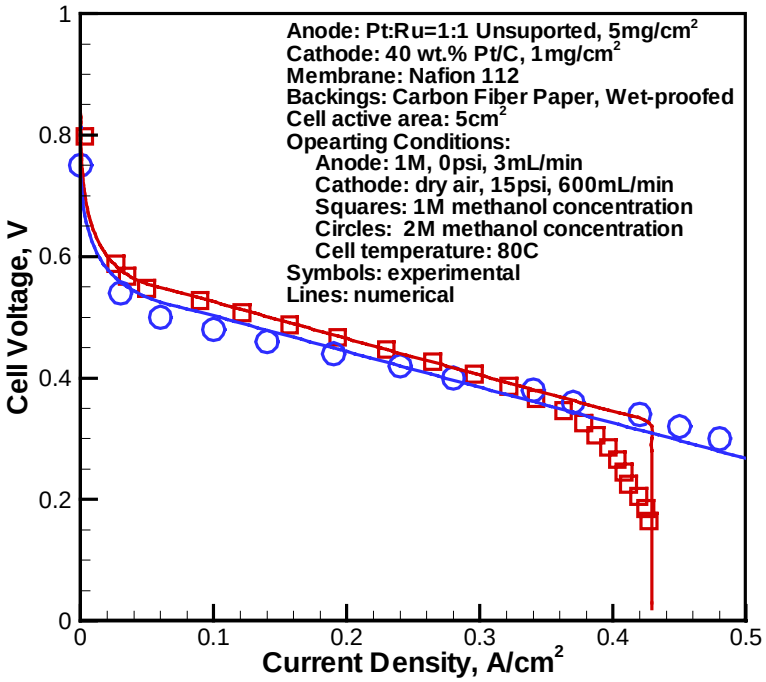

Figure 11 Validation of the present DMFC model with the experimental data of a 5cm^2 cell at different methanol feed concentrations

In Proc of Direct Methanol Fuel Cell Symposium, 199th Electrochem.l Soc. Mtg, Washington DC, 3/01.

Key Words:
Direct methanol fuel cells; Mathematical modeling; Methanol crossover; Mixed potential; Two-phase transport; Computational fluid dynamics.